FRONTIERS OF PHYSICS

RESEARCH ARTICLE
Volume 18 / Issue 3 / 33301 / 2023

Au/MXene based ultrafast all-optical switching

Yule Zhang[1], Feng Zhang[1], Bowen Du[1], Hualong Chen[1], S. Wageh[2], Omar A. Al-Hartomy[2], Abdullah G. Al-Sehemi[3], Bin Zhang[1,†], Han Zhang[1,‡]

1 International Collaborative Laboratory of 2D Materials for Optoelectronics Science and Technology of Ministry of Education, Institute of Microscale Optoelectronics and Translational Medicine, The First Affiliated Hospital (Shenzhen Second People's Hospital), College of Physics and Optoelectronic Engineering, Shenzhen University, Shenzhen 518060, China
2 Department of Physics, Faculty of Science, King Abdulaziz University, Jeddah 21589, Saudi Arabia
3 Research Center for Advanced Materials Science (RCAMS), King Khalid University, P.O. Box 9004, Ab-ha, 61413, Saudi Arabia
Corresponding authors. E-mail: †00910023@pku.edu.cn, ‡hzhang@szu.edu.cn
Received September 1, 2022; accepted December 1, 2022

ABSTRACT

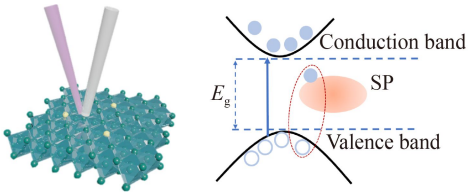

All-optical switches have arisen great attention due to their ultrafast speed as compared with electric switches. However, the excellent optical properties and strong interaction of two-dimensional (2D) material MXene show great potentials in next-generation all-optical switching. As a solution, we propose all-optical switching used Au/MXene with switching full width at half maximum (FWHM) operating at 290 fs. Compared with pure MXene, the Au/MXene behaves outstanding performances due to local surface plasmon resonance (LSPR), including broadband differential transmission, strong near-infrared on/off ratio enhancement. Remarkably, this study enhances understanding of Au/MXene based ultrafast all-optical switching red-shifted about 34 nm in comparison to MXene, validating all optical properties of Au/MXene opening the way to the implementation of optical interconnection and optical switching.

Keywords Au/MXene, ultrafast all-optical switching, Au/MXene carrier lifetime

1 Introduction

Over the last decade, the family of two-dimensional (2D) materials, including graphene, layered transition-metal dichalcogenides (TMDCs), black phosphorus, as well as MXene, have been reported due to their marvelous electrical, thermal, and optical properties [1–5]. Basically, 2D materials and ultrafast photonic devices show the saturable absorption [6], optical Kerr effect [7] and so on. Recently, there has been traditionally attracted considerable interest in MXene. The general composition of MXene is $M_{n+1}AX_n$, where M is a transition metal (such as Ti, Zr, Nb, V, Ta or Mo), X symbolizes C and/or N, A is the main group element (such as Al or Si), and n equals to 1, 2, or 3. Usually, Al or Si atoms are substituted with functional groups, which serve as surface termination units T (e.g., –O, –OH, –F), representing the $M_{n+1}X_nT_x$ nanosheet (n = 1, 2, or 3) [8]. According to the high density of states at the Fermi level, MXene $Ti_3C_2Cl_x$ has fascinating transport properties, including high mobility and on-off ratios in vertical tunnelling transistors, due to its high density of states at the Fermi level [9]. Since the optical properties of MXene are referred to as their band structures [8, 10], They would be used in a variety of optical applications, including all-optical modulators. High-performance MXene with more than 90% broadband optical transmittance is rapidly garnering attention as promising materials in a wide range of research domains, demonstrating significant potential as new members of the two-dimensional family.

MXene is expected to be a new generation photoelectric

*Special Topic: MXene and Its Applications (Eds.: Qing Huang, Ju Han Lee & Guangcun Shan).

Higher Education Press

https://doi.org/10.1007/s11467-022-1248-0

material due to the small gap and broadband saturable absorption capability. Such materials have several locations for metal atoms thanks to the thin-layer structure. Furthermore, the strong contacts that are stable under physical inspection and the active center's unsaturated coordination state are the sources of the performance of metal-anchored 2D materials [11]. It has been shown that ultrathin two-dimensional MXene nanosheets may stabilize metal species such as metal nanoparticles, nanoclusters or single atoms. Comparing to other MXene van der Waals (vdW) heterostructures, it has the possibilities for reduced power consumption and enhanced efficiency [12]. The potential optical features of layered materials have, however, in recent years generated a great deal of interest in optical switches.

Ultrafast processing of the date requires ultrafast switches, which is an essential part of transmission conditions. Owing to graphene's strong optical nonlinear absorption and switch time of 260 fs, ultrafast all-optical switching has been performed in graphene. Transient absorption (TA), a potential tool that does not rely on the emission of photons or photoelectrons, has recently emerged as an all-optical approach to investigate the potential uses of MXene in optical switches by examining the dynamic of carriers over short timescales. Fundamentally, we reported the carrier dynamics study of MXene in all-optical switches, which is widely employed in the ultrafast laser and light modulator with fast carrier relaxation.

In this work, Au nanoparticles anchored MXene were proposed to study ultrafast all-optical switching. Additionally, the creation of high-energy electrons generated by local surface plasmon resonance is the determining factor of the energy transfer between the plasmon-metal nanoparticles and the semiconductor (LSPR). To date, free-space laser contact with materials has allowed for the universal realization of LSPR excitation in Au particles. The impact of LSPR excitation, ultrafast transmission, and broadband differential transmission can be used as tunable switches in integrated circuits and optical communication systems. We discovered that Au/MXene is a material that shows promise in the realm of optical communication.

2 Results and discussion

2.1 Synthesis of Au/MXene

In a typical synthetic process, 100 mg MXene $Ti_3C_2Cl_x$ was firstly dispersed in 10 mL ultrapure water under vigorous stirring, followed by the addition of 1 mg, 0.1 M NaOH aqueous solution to adjust the pH to 9. Afterwards, 0.1 mL, 0.1 M $HAuCl_4$ solution were added to the MXene dispersion, followed by stirring for another 5 h at 4 ℃ under ice bath. The resulting solution was filtered to remove the supernatant, and the obtained precipitate was washed with ultrapure water 3 times and dried in a vacuum oven at 60 ℃ for 12 h. The dried sample was then loaded in a quartz tube, calcined at 160 ℃ for 1 h in 5% H_2/Ar flow (40 mL/min). Afterward, the sample was dispersed in water via sonication.

2.2 Characterization

Metal content in the catalyst was determined by iCAP 6000 series inductively coupled plasma optical emission spectrometry (ICP-OES). The catalysts were digested in aqua regia (HCl/HNO_3 = 3:1) at 353 K for 4 h and then diluted with deionized water to a certain volume before analysis. The morphologies were observed by transmission electron microscopy (HAADF-STEM and EDX; FEI, Titan Cubed Themis G201, 300 kV) and JEM-F200. Hydrodynamic diameter (Dh) and polydispersity index (PDI) were determined by the dynamic light scattering (DLS) techniques using a Malvern Zetasizer Nano-ZS instrument (ZEN3600, Malvern Instruments) equipped with a temperature controller and a 633 nm He–Ne laser at a scattering angle of 173° at 25 °C. XPS spectrum was collected on an X-ray photoelectron spectrum (ESCALAB 250, Thermo Fisher, USA). The X-ray absorption fine structure spectra (XAFS) Au L_3-edge were collected at BL07A1 beamline of National Synchrotron Radiation Reaearch Center (NSRRC). The data were collected in fluorescence mode using a Lytle detector while the corresponding reference sample were collected in transmission mode. The sample was grinded and uniformly daubed on the special adhesive tape. The obtained XAFS data was processed in Athena (Version 0.9.26) for back-ground, pre-edge line and post-edge line calibrations. Then Fourier transformed fitting was carried out in Artemis (Version 0.9.26). The k_3 weighting, k range of 3–14 $Å^{-1}$ and R range of 1–~3 Å were used for the fitting of Co foil; k range of 3–11 $Å^{-1}$ and R range of 1–~2 Å were used for the fitting of samples. The four parameters, coordination number, bond length, Debye–Waller factor and E_0 shift (CN, R, ΔE_0) were fitted without anyone was fixed, the σ_2 was set. For Wavelet Transform analysis, the $\chi(k)$ exported from Athena was imported into the Hama Fortran code. The parameters were listed as follow: R range, 1–4 Å, k range, 0–12 $Å^{-1}$ for samples; k weight, 3; and Morlet function with κ = 10, σ = 1 was used as the mother wavelet to provide the overall distribution.

As shown in Fig. 1(a), TEM proves Au nanoparticles with a size of 3–5 nm are well dispersed on the MXene surface and zoom in to see they anchor on the surface tightly. To further determine the atomic components and corresponding rate of the Au/MXene nanosheets, EDX-mapping proves Au species are well distributed on the MXene surface in Figs. 1(b)–(e).

X-ray absorption spectroscopy (XAS) analysis was performed for further checking the electronic structures

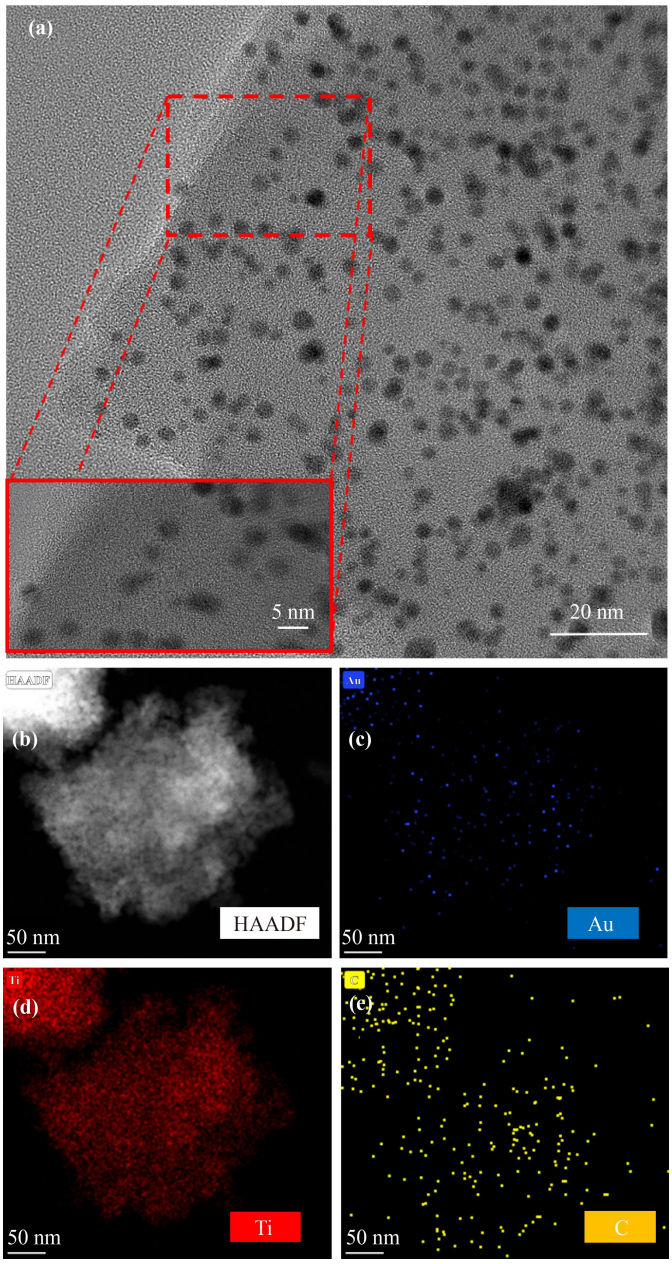

Fig. 1 Morphology characterizations of straticulate Au/MXene **(a)** Transmission Electron Microscope (TEM) images of scale bar: 20 nm and 5 nm. **(c–e)** Au, Ti, and C EDS-mappings in **(b)** HAADF EDX-mapping.

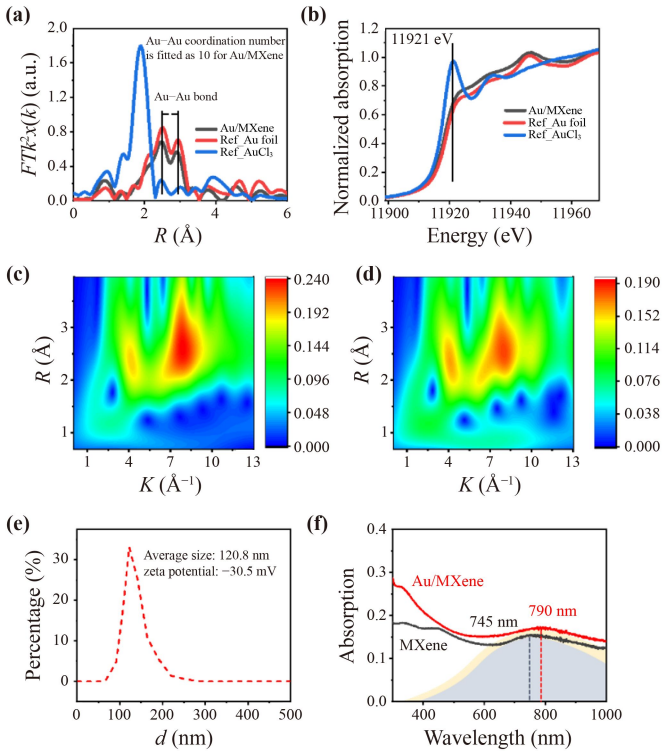

Fig. 2 **(a)** XANES and **(b)** EXAFS results of Au foil, $AuCl_3$ standards and Au/MXene. **(c, d)** Wavelet transform of Au L_3 edge EXAFS in Au/MXene. **(e)** DLS spectrum of Au/MXene. **(f)** UV-vis absorption spectra of Au/MXene and MXene.

and directly investigating the coordinating environment of Au species in Au/MXene. Notably, in the X-ray absorption near-edge structure (XANES) spectrum [Fig. 2(a)], the white-line intensity of Au at 11921 eV in Au/MXene is higher than that of $AuCl_3$, and closer to that of Au foil standard. Estimation of the average Au valence for our sample is +0.5. The positively charged Au suggests electronic interaction between Au and MXene via coordination. Extended X-ray absorption fine structure spectroscopy (EXAFS) in Fig. 2(b) provided key evidence for the local environment of Au species. It is found that in the EXAFS and Wavelet transform spectra [Figs. 2(c, d)], almost no Au–Cl contribution at ~2.00 Å was observed in the k_3-weighted EXAFS at Au L_3 edge of Au/MXene, and the Au–Au contribution at around 2.85 Å dominated. This demonstrates that the chloride ligands in the precursor $HAuCl_4$ have been completely removed and Au probably interacts with MXene through the coordination Au–C–Ti, which modulates the electronic structures of Au and MXene and endow the sample with promising optoelectronic properties.

To confirm whether the optical absorption identified for Au/MXene and pristine MXene, we test dynamic light scattering (DLS) and the UV-vis-IR absorption spectrometer for both. The size of Au/MXene in DLS results was approximately 120.8 nm for diameter in Fig. 2(e). Pure MXene exhibits broadband absorption, which has been reported in other literature [13]. Light absorption is enhanced after Au modification. As shown in Fig. 2(f), the center spectroscopy of transversal SP mode is about 745 nm and 790 nm [14].

2.3 Ultrafast optical switching

MXene is sufficient for the operating bandwidth of an ultrafast optical switch since it has a short photocarrier

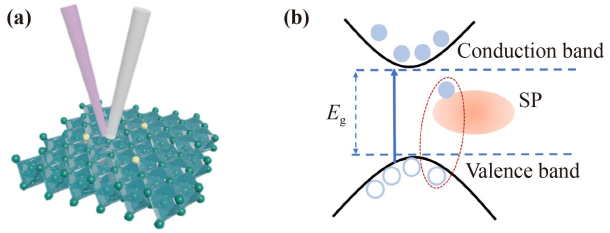

Fig. 3 Schematic representation of structure of the optical switch. **(a)** Photoexcited Au/MXene by pump light and probe light. **(b)** Electron was excited from ground state to excited state.

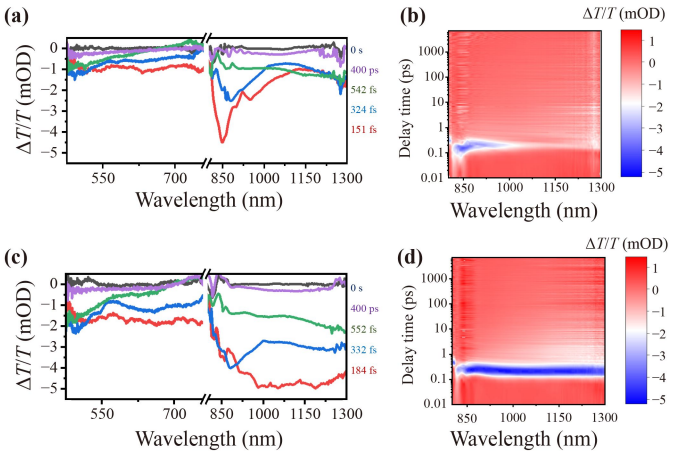

Fig. 4 MXene and Au/MXene TA spectrums. **(a)** Selective pump-probe delay times of MXene film on quartz in the probe range (475–780 nm and 800–1300 nm) by 420 nm excitation. **(b)** MXene 2D TA spectrum map with excitation intensity of 0.5 J/pulse. **(c)** Au/MXene film on quartz in the same probe. **(d)** 2D TA spectrum map of Au/MXene in the same pulse energy.

lifetime. The carrier concentration and lifetimes provide a strict regime on switching speed. The most recent study used an ultrafast pump-probe to examine how doping affected the carrier dynamics in MXene. We create and optically control ultrafast switching in Au/MXene at room temperature via the strong photon–electron effect.

Moreover, we estimate relaxation time in MXene as a comparison. Exploring the structural changes caused by the excitation of Au/MXene employing time resolved pump probe diffraction throughout. At the same optical excitation by 420 nm pump light, we demonstrate enhanced optical modulation speed due to photocarrier relaxation dynamics in Au/MXene. The novel integrated modulation requires a large optical bandwidth in addition to high modulation speed.

Pump-probe scheme of an all-optical switch is shown in Fig. 3. If we studied MXene with a bandgap of 1.2 eV using the pump-probe technique with femtosecond resolution, we revealed substantial evidence of ultrafast relaxation time. The pump light at 420 nm as well as probe spectrum of 480–760 nm and 800–1300 nm were generated by injecting different crystals through complex nonlinear processes. The delay line can adjust the delay between the two laser beams, resulting in the creation of a free carrier for combining electrons and holes in Fig. 3(b). The process from ground state to excited state and excited state to ground state was defined as ultrafast switching. Herein, in order to investigate the all-optical switching properties between MXene and Au/MXene, a TA spectroscopy with a pump wavelength of 420 nm (2.95 eV) was used to detect wavelength from the visible to the near-infrared. In addition, the temporal resolution between the pump pulse and probe pulse is 150 fs, and the probe pulse signal is detected using a silicon-based Complementary Metal Oxide Semiconductor (CMOS) linear image sensor. A dynamic time-resolved TA spectral signal can be obtained by analyzing the pulse delay time between the emitted probe beam and the pump beam.

As shown in Figs. 4(a) and (c), the $\Delta T/T$ (mOD) in y axial presents the broadband differential transmission responses of probe light at pulse energy of 500 nJ as a function. The different delay times have been marked in the graph. The pump light passes through the film as the electrons in the ground state transition to the excited state, and the absolute value of the signal strength shows the intensity of electrons in the excited state.

Meanwhile, the delay times of MXene and Au/MXene reaching the maximum of electron concentration in the excited state are around 151 fs and 184 fs, respectively. We investigate Au nanoparticles on modulation depth as they decrease MXene transmission rate. Concentrate on different carrier dynamics of other 2D materials [6], such as graphene [15], black phosphorus [16], and MoS_2 [17], MXene has an ultrafast modulation speed and could be utilized in optical switches or ultrafast modulators in the future. Then we investigate whether the existence of Au nanoparticles can significantly decrease the transmission signal by comparing the differential transmission signal of Figs. 4(b) and (d). There is a doubling absorption pattern in the visible light range for delay times that are similar. It is exciting to see that there is a noticeable difference in the near-infrared. Experiments have shown that Au atoms can trap most of the photogenerated carriers at the femtosecond scale and then release them to defect locations on the MXene surface, where the trapped electrons and holes decay on the femtosecond, and the Au atoms lead to a buildup with the carriers through electrostatic and covalent bonding, where significant charge transfer occurs between the heterogeneous structure. The conduction band electrons on the local surface plasmon resonance of metal nanoparticles, initially 1–100 fs, generate free carriers through Landau damping and other photoelectron interactions, forming

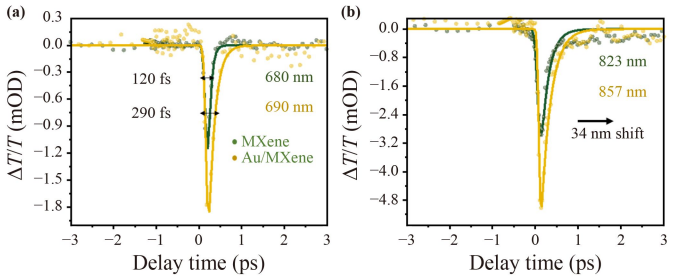

Fig. 5 MXene and Au/MXene carrier liftimes. **(a)** Ultrafast dynamics observed at 680 and 690 nm. **(b)** At the probe wavelength of 823 nm and 857 nm.

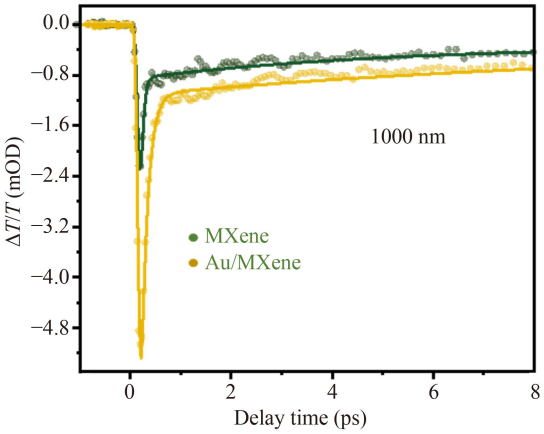

Fig. 6 Ultrafast dynamics at the probe wavelength of 1000 nm.

Table 1 Carrier delay time at probe wavelength of 1000 nm.

Materials	τ_1	τ_2	τ_3
MXene	40.69 fs ± 6 fs	2.92 ps ± 12 fs	320.8 ps ± 5 ps
Au/MXene	125.7 fs ± 7 fs	10.64 ps ± 30 fs	4.73 ns ± 90 ps

carrier energies following the Planck distribution [18]. With its ultrafast modulation speed, Au/MXene is compatible with the current generation of near-infrared modulators for optical communication.

Furthermore, we thoroughly discuss carrier delay times at various wavelengths in order to reveal carrier movement for better application in all-optical switches. As illustrated in Fig. 5(a), we used an exponential function [$\Delta T/T = A \exp(-t/\tau)$], where A represents the component amplitudes, "t" represents the delay time between the pump-probe light, and τ corresponds to the carrier lifetime, to fit the dynamic curves.

It demonstrates that the carriers lifetime constants of MXene and Au/MXene are fitted to be 63.2 ± 8 fs and 145.5 ± 8 fs close to first-order exponential fit at about 685 nm. After reaching the surface of the Au nanoparticle and remaining in an excited thermal state for around ~10 fs, the high-energy electrons stimulated by the local surface plasmon resonance will instantly pump into the MXene conduction band [19].

Besides, the $\Delta T/T$ curves provide a useful representation of the full width at half maximum (FWHM), which has been measured at 120 fs and 290 fs, suggesting that it may find use on the near-infrared all-optical switches. The result shows an important trade-off relationship between MXene and Au/MXene, while Au/MXene shows a slower time than bare MXene, it has a larger modulation signal. In Fig. 5(b), they are fitted to be 182.5 ± 9 fs in 823 nm and 239.1 ± 6 fs in 857 nm. The rise in the imaginary portion of the metal's dielectric constant creates a red-shift in the local surface plasmon resonance, which is directly caused by the change in the conduction band electron distribution function [20]. It demonstrates the device's incredibly quick switching-on and switching-off processes [21, 22]. In addition, we further argued that the sample's optical switching cut-off wavelength has been red-shifted as a result of the presence of Au nanoparticles. Based on the multilayer spherical model with an effective middle layer, scattering by the Mie theory actually occurs. In order to allow the particle spheres to absorb the dispersed light in the near-field of photons with varied degrees of red-shift approximately 34 nm (857–890 nm) in near-infrared, an Au/MXene surface has been built [23, 24].

As shown in Fig. 6, three-exponential function has been used to fit the dynamic curves [$\Delta T/T = A_1\exp(-t/\tau_1) + A_2\exp(-t/\tau_2) + A_3\exp(-t/\tau_3)$].

According to measurements, the electron distributions under conditions of excitation of electrons transmission are shown in Table 1 as carrier–carrier (τ_1) and carrier-phonon scattering (τ_2) and phonon–phonon scattering (τ_3). The pump light is trapped by Au nanoparticles attached on MXene, increasing the modulation ratio of the surrounding MXene for the probe light. Au/MXene has a longer delay time at τ_1 and τ_2, which illustrates the deeper modulation and higher carrier lifetime are displayed due to the local plasmon increased excitation, in addition to the band gap reorganization that occurred after τ_1 [20]. The near-infrared wavelength indicate that Au/MXene exhibits the optical switches have become a result of the on/off ratio.

3 Methods

3.1 Preparation and modification

To date, many methods, including mechanical cleavage, liquid exfoliation, chemical vapor deposition, and wet chemistry methods, have been developed to prepare 2D nanomaterials. For MXene, it is mainly used top-down methods to synthesize. Moreover, in order to improve the aqueous stability, various strategies have been

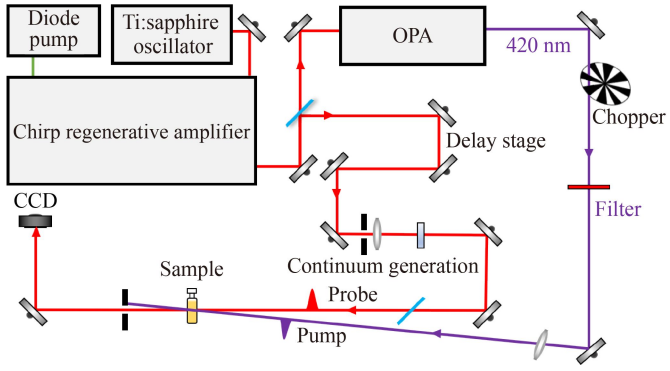

Fig. 7 A typical pump-probe experimental set-up.

adopted to modify them for a wide range of photonics applications. In a typical synthetic process, 100 mg of MXene $Ti_3C_2Cl_x$ was firstly dispersed in 10 mL ultrapure water under vigorous stirring, followed by the addition of 1 mg of 0.1 M NaOH aqueous solution to adjust the pH to 9. Afterward, 0.1 mL of 0.1 M $HAuCl_4$ solution was added to the MXene dispersion, followed by stirring for another 5 h at 4 ℃ under an ice bath. The resulting solution was filtered to remove the supernatant and the obtained precipitate was washed with ultrapure water 3 times and dried in vacuum oven at 60 ℃ for 12 h. The dried sample was then loaded in a quartz tube, and calcined at 160 ℃ for 1 h in 5% H_2/Ar flow (40 mL/min). Afterwards, the sample was dispersed in water via sonication.

3.2 Pump-probe technique

Typically, as shown in Fig. 7, there are three stages. First, at a typical repetition rate of 1 kHz, a mode-locked Ti:sapphire 800 nm oscillator generates ~45 fs, 1–3 mJ·pulse^{-1} pulses. Second, the femtosecond pulses were split for the pump and probe. The pump light passed through an OPA that was employed to probe the carrier dynamics in the sample, and the probe light was delayed by a motorized linear stage that can be placed in either beam path and modulated by a continuum generation stage. Finally, two beams were focused on the sample with a lens. The pump beam was blocked after the sample was transmitted, and the CCD detected the probe light.

4 Conclusions

We proposed engineering on 2D semiconductor MXene by anchoring Au nanoparticles with a size of 3–5 nm. XANES and EXAFS were used to check the electronic structures and investigate the coordinating environment of Au species in Au/MXene. We used TA spectra to analyze an emerging switching of FWHM in Au/MXene based on experimental results, according to absorption spectra of Au/MXene and MXene, the center spectra 790 nm and 745 nm (290 fs). Furthermore, the Au/MXene exhibits outstanding performance in the near-infrared wavelength with the switching red-shift 34 nm. This work refers to all-optical properties for meeting optical devices.

Acknowledgements The research was partially supported by the funding of the Science and Technology Development Fund (Grant Nos. 007/2017/A1 and 132/2017/A3), Macao Special Administration Region (SAR), China, and the National Natural Science Fundation of China (Grant Nos. 61875138, 61435010, and 6181101252); King Khalid University through Research Center for Advanced Materials Science (RCAMS) (Grant Nos. RCAMS/KKU/006/21); and the Technology Innovation Commission of Shenzhen (Grant Nos. KQTD2015032416270385, JCYJ20150625103619275, JCYJ20170811093453105, KCXFZ20201221173413038, and JCYJ20190806163805286).

References

1. S. Z. Butler, S. M. Hollen, L. Cao, Y. Cui, J. A. Gupta, H. R. Gutiérrez, T. F. Heinz, S. S. Hong, J. Huang, A. F. Ismach, E. Johnston-Halperin, M. Kuno, V. V. Plashnitsa, R. D. Robinson, R. S. Ruoff, S. Salahuddin, J. Shan, L. Shi, M. G. Spencer, M. Terrones, W. Windl, and J. E. Goldberger, Progress, challenges, and opportunities in two-dimensional materials beyond graphene, *ACS Nano* 7(4), 2898 (2013)
2. A. K. Geim and I. V. Grigorieva, Van der Waals heterostructures, *Nature* 499(7459), 419 (2013)
3. A. N. Grigorenko, M. Polini, and K. S. Novoselov, Graphene plasmonics, *Nat. Photonics* 6(11), 749 (2012)
4. J. W. Jiang and H. S. Park, Negative Poisson's ratio in single-layer black phosphorus, *Nat. Commun.* 5(1), 4727 (2014)
5. Q. H. Wang, K. Kalantar-Zadeh, A. Kis, J. N. Coleman, and M. S. Strano, Electronics and optoelectronics of two-dimensional transition metal dichalcogenides, *Nat. Nanotechnol.* 7(11), 699 (2012)
6. Z. Q. Luo, Y. Huang, M. Zhong, Y. Li, J. Wu, B. Xu, H. Xu, Z. Cai, J. Peng, and J. Weng, 1-, 1.5-, and 2-μm fiber lasers Q-switched by a broadband few-layer MoS_2 saturable absorber, *J. Lightwave Technol.* 32(24), 4079 (2014)
7. L. M. Wu, Y. Dong, J. Zhao, D. Ma, W. Huang, Y. Zhang, Y. Wang, X. Jiang, Y. Xiang, J. Li, Y. Feng, J. Xu, and H. Zhang, Kerr nonlinearity in 2D graphdiyne for passive photonic diodes, *Adv. Mater.* 31(14), 1807981 (2019)
8. X. T. Jiang, A. V. Kuklin, A. Baev, Y. Q. Ge, H. Ågren, H. Zhang, and P. N. Prasad, Two-dimensional MXenes: From morphological to optical, electric, and magnetic properties and applications, *Phys. Rep.* 848, 1 (2020)
9. L. Wu, X. Jiang, J. Zhao, W. Liang, Z. Li, W. Huang, Z. Lin, Y. Wang, F. Zhang, S. Lu, Y. Xiang, S. Xu, J. Li, and H. Zhang, MXene-based nonlinear optical information converter for all-optical modulator and switcher, *Laser Photonics Rev.* 12(12), 1800215 (2018)

10. Y. L. Bai, K. Zhou, N. Srikanth, J. H. L. Pang, X. He, and R. Wang, Dependence of elastic and optical properties on surface terminated groups in two-dimensional MXene monolayers: A first-principles study, *RSC Adv.* 6(42), 35731 (2016)
11. G. Kyriakou, M. B. Boucher, A. D. Jewell, E. A. Lewis, T. J. Lawton, A. E. Baber, H. L. Tierney, M. Flytzani-Stephanopoulos, and E. C. H. Sykes, Isolated metal atom geometries as a strategy for selective heterogeneous hydrogenations, *Science* 335(6073), 1209 (2012)
12. H. Yuan and Z. Y. Li, Interfacial properties of black phosphorus/transition metal carbide van der Waals heterostructures, *Front. Phys.* 13, 138103 (2018)
13. F. Zhang, R. Cao, Z. Li, S. Gao, H. Chen, J. Guo, Y. Zhang, B. O. Al-Amoudi, S. Wageh, A. A. Al-Ghamdi, X. Zhang, and H. Zhang, Dynamics of broadband photoinduced species and enabled photodetection in MXenes, *Nanophotonics* 11(13), 3139 (2022)
14. J. K. El-Demellawi, S. Lopatin, J. Yin, O. F. Mohammed, and H. N. Alshareef, Tunable multipolar surface plasmons in 2D Ti_3C_2TX MXene flakes, *ACS Nano* 12(8), 8485 (2018)
15. L. B. Huang, G. V. Hartland, Luxmi, R. M. Feenstra, C. Lian, K. Tahy, and H. Xing, Ultrafast transient absorption microscopy studies of carrier dynamics in epitaxial graphene, *Nano Lett.* 10(4), 1308 (2010)
16. W. Z. Wu, Y. Zhou, J. Wang, Y. Shao, D. Kong, Y. Gao, and Y. Wang, The pump fluence and wavelength-dependent ultrafast carrier dynamics and optical nonlinear absorption in black phosphorus nanosheets, *Nanophotonics* 9(7), 2033 (2020)
17. L. Wibmer, S. Lages, T. Unruh, and D. M. Guldi, Excitons and trions in one-photon- and two-photon-excited MoS_2: A study in dispersions, *Adv. Mater.* 30(12), 1706702 (2018)
18. C. Zhan, X. J. Chen, J. Yi, J. F. Li, D. Y. Wu, and Z. Q. Tian, From plasmon-enhanced molecular spectroscopy to plasmon-mediated chemical reactions, *Nat. Rev. Chem.* 2(9), 216 (2018)
19. A. Furube, L. Du, K. Hara, R. Katoh, and M. Tachiya, Ultrafast plasmon-induced electron transfer from gold nanodots into TiO_2 nanoparticles, *J. Am. Chem. Soc.* 129(48), 14852 (2007)
20. X. L. Wang, R. Morea, J. Gonzalo, and B. Palpant, Coupling localized plasmonic and photonic modes tailors and boosts ultrafast light modulation by gold nanoparticles, *Nano Lett.* 15(4), 2633 (2015)
21. Y. Yang, J. Ward, and S. N. Chormaic, Quasi-droplet microbubbles for high resolution sensing applications, *Opt. Express* 22(6), 6881 (2014)
22. X. F. Han, Y. X. Weng, R. Wang, X. H. Chen, K. H. Luo, L. A. Wu, and J. Zhao, Single-photon level ultrafast all-optical switching, *Appl. Phys. Lett.* 92(15), 151109 (2008)
23. N. Zhang, C. Han, Y. J. Xu, J. J. IV Foley, D. Zhang, J. Codrington, S. K. Gray, and Y. Sun, Near-field dielectric scattering promotes optical absorption by platinum nanoparticles, *Nat. Photonics* 10(7), 473 (2016)
24. G. Mie, Contributions to the optics of turbid media, particularly of colloidal metal solutions, *Ann. Phys.* 25(3), 377 (1908)